JOURNAL OF PROPULSION AND POWER
Vol. 25, No. 2, March–April 2009

Comparison of Several Zero-Boil-Off Pressure Control Strategies for Cryogenic Fluid Storage in Microgravity

Charles H. Panzarella*
Equity Engineering Group, Shaker Heights, Ohio 44122
and
Mohammad Kassemi†
NASA John H. Glenn Research Center at Lewis Field, Cleveland, Ohio 44135

DOI: 10.2514/1.35611

Four different tank pressure control strategies based on various combinations of active cooling and/or forced mixing are investigated numerically. The first, and most effective, strategy uses a subcooled liquid jet to simultaneously mix and cool the bulk liquid. The second strategy is based on separate mixing and cooling via a forced uncooled liquid jet and an independent cold finger. The third strategy uses a cold finger alone with no forced mixing. Finally, the fourth strategy examines the effect of mixing alone without any active cooling. Detailed numerical solutions are obtained for each case by solving the Navier–Stokes and energy equations in the liquid region coupled to a lumped heat and mass treatment of the vapor region. It is shown that the most rapid and effective means of countering self-pressurization is achieved with a subcooled liquid jet. In the case of separate mixing and cooling, the pressure can still be reduced, but over a much longer period of time. Finally, cooling without any forced mixing is able to limit the pressure rise, but not very effectively, although for long-duration storage in which rapid pressure control is not required, this may still constitute a viable approach. While presenting the results of the various simulation case studies, an in-depth comparative analysis of transport phenomena associated with each case is also performed from which salient engineering recommendations are derived for optimization of the zero-boil-off design.

Nomenclature

A	=	surface area, cm/s^2
a	=	tank acceleration, cm/s^2
Bi	=	diffusive Biot number, $q_v R_v / k_v T_s$
Bi_δ	=	convective Biot number, $q_v \delta / k_v T_s$
c	=	specific heat, erg/K · g
Gr	=	Grashof number, $a\rho_l^2 \beta_l q_w R_t^4 / k_l \mu_l^2$
h	=	height of jet fluid reservoir, cm
k	=	thermal conductivity, erg/cm · s · K
L	=	latent heat of vaporization, erg/g
m	=	molar mass, g/mol
p	=	pressure, atm
Q	=	net heat flow, W
q	=	heat flux, W/cm^2
R	=	spherical radius, cm
R_g	=	ideal-gas constant, erg/K · mol
r	=	radial cylindrical coordinate, cm
T	=	temperature, K
t	=	time, s
V	=	volume, cm^3
u	=	flow speed, cm/s
z	=	axial cylindrical coordinate, cm
α	=	thermal diffusivity, cm^2/s
β	=	thermal expansion coefficient, 1/K
δ	=	thermal boundary-layer thickness, $\sqrt{\alpha_v / u_j R_v}$
μ	=	dynamic viscosity, g/cm · s
ρ	=	density, g/cm^3
σ	=	surface tension, dyne/cm

Subscripts

b	=	normal boiling point
c	=	convective
d	=	diffusive
h	=	heater
j	=	jet
l	=	liquid
min	=	minimum
max	=	maximum
n	=	nozzle
o	=	outer
s	=	saturation
t	=	total/tank
v	=	vapor
w	=	wall

Received 16 November 2007; revision received 26 August 2008; accepted for publication 27 August 2008.

*Group Head, Applied Mechanics, 20600 Chagrin Boulevard; chpanzarella@equityeng.com.
†Chief Fluids Scientist, National Center for Microgravity Research, 21000 Brookpark Road, Mailstop 110-3; mohammad.kassemi@nasa.gov. Member AIAA.

I. Introduction

THE extension of human space exploration from low Earth orbit into the further reaches of the solar system is one of NASA's biggest challenges for the next millennium. The projected exploration programs include a series of human and robotic expeditions to low and high Earth orbits, the moon, Mars, and possibly the asteroids and other planetary moons.

With the exception of extremely-short-duration missions, significant cost savings can be achieved if the launch mass is reduced by improving the cryogenic storage and transfer technologies [1]. Cryogen vaporization is one of the main causes of self-pressurization of the storage tanks and leads to undesirable mass loss due to the inevitable need for venting to reduce the storage tank pressure. Vaporization can occur during the filling process or may be caused by heat leaks into the tank from the surrounding environment. For on-surface applications, such as those on the

surface of the Earth, moon, or Mars, the spatial configuration of liquid and vapor is dictated by gravity and is well known. In this situation, continuous venting can be easily accomplished, but it results in considerable cryogen mass loss over time. For in-space applications, the spatial configuration of liquid and vapor is generally unknown, and direct venting without prepositioning of the two phases is precluded due to the possibility of expelling liquid along with the vapor. Moreover, venting in space is also undesirable because it prohibits or endangers manned flight operations around the storage tanks.

In short, from both safety and mass loss perspectives, a ventless pressure control strategy is highly desirable for both on-surface and in-space applications. The zero-boil-off (ZBO) pressure control strategy has been proposed as a possible means of achieving ventless storage through the synergetic application of active cooling and forced mixing [2]. The ZBO goals can be accomplished by using cryocoolers along with impellers, liquid jets, or spray bars. However, optimization of the ZBO design can be extremely complex and requires hand-in-hand experimental and theoretical elucidation of the associated transport phenomena.

The self-pressurization of cryogen storage tanks has been the subject of considerable previous experimental investigations (see Panzarella and Kassemi [3] for a comprehensive review), but few have directly focused on the effects of the reduced-gravity environment. One important study is due to Aydelott [4], who shows that the initial rate of pressurization is lower under reduced-gravity conditions than on the ground. This was primarily attributed to an increase in the tank-wall surface area covered by the liquid. Other aspects of cryogen storage have also been considered, such as the effect of a liquid jet on the bulk mixing behavior [5,6] and its ability to control the tank pressure [7] and reduce thermal stratification [8].

Previous numerical studies of tank pressurization have been primarily limited to purely thermodynamic treatments [9–11], fluid flow, and thermal stratification in the liquid, without any consideration of the resultant pressure rise in the vapor [12–17] or the evolution of the phase distribution without any thermal considerations [18–25].

Panzarella and Kassemi [3] developed a more comprehensive numerical model by coupling a lumped-energy and lumped-mass approximation of the vapor region with a direct numerical solution of the Navier–Stokes, energy, and continuity equations in the liquid region. This approach has already been used to investigate the pressurization of a small ground-based tank as well as large spherical tanks in both zero-gravity and microgravity environments [26]. The results of these studies indicate that the initial rate of pressurization depends on the characteristics of the heat, mass, and momentum transport in the bulk liquid as influenced by the particular heat-flux distribution on the tank wall even though the final rate of pressurization agrees with predictions provided by a purely thermodynamic description.

Panzarella et al. [27] have also used this model to demonstrate the effectiveness of a laminar subcooled liquid jet in controlling the tank pressure. Despite the apparent effectiveness of the subcooled liquid jet, it may not always be possible or efficient to provide or sustain this mode of rapid cooling for long periods of time due to engineering limitations, power-consumption requirements, and the possibility of mechanical failure. Consequently, this paper will investigate several alternative strategies for pressure control and compare their effectiveness to the performance of the subcooled-jet mixing case.

The strategies that are considered here primarily involve a separation of the cooling and mixing mechanisms in different fashions. First, an uncooled liquid jet will be used along with a separate cold finger placed at various locations against the tank wall. Next, the effectiveness of cooling without any forced mixing will be examined. Finally, the performance of forced mixing via a liquid jet but without any cooling will be assessed to demonstrate the effect of disrupting the thermal stratification of the bulk liquid. The results will show that none of these strategies are able to reduce the tank pressure as rapidly as the subcooled liquid jet, which can be regarded as a standard for comparison of the different pressure control schemes. However, for long-duration storage in which rapid pressure control is not required, these alternative approaches may find favorable application due to their lower power-consumption requirements.

II. Cryogenic Tank Model

Consider a large spherical tank in microgravity mostly filled with liquid hydrogen (95% by volume) and its vapor, as shown in Fig. 1. A cylindrical coordinate system is used to describe the model with the origin at the center of the tank and with the z axis parallel to the direction of the average residual acceleration vector. The solution is assumed to be axisymmetric about this axis. It was shown previously in [26] that even in microgravity the ullage rises in a direction opposite to the direction of the residual tank acceleration vector and reaches one side of the tank quite rapidly in comparison with the other relevant timescales of this problem. Thus, in the present model that is concerned with long-duration storage, the vapor region is assumed to remain spherical with a fixed volume (volume changes due to evaporation are quite small and can be neglected) and is stationary at one side of the tank, with a 1-mm-thick layer of liquid between the vapor and the tank wall at its closest point. Even though the vapor region is fixed, fluid is still allowed to flow over its boundary by imposing a zero tangential-stress boundary condition.

This particular thickness of the liquid film (1 mm) was chosen somewhat arbitrarily, but small enough to simulate the vapor being in direct contact with the wall without having to deal with any contact-line issues. The heat flux at any point through a sufficiently thin layer will be nearly constant (because the temperature profile is almost linear) and equal to the heat flux imposed on the tank wall. Thus, the wall heat flux is imparted directly to the liquid–vapor interface just as if the vapor were in direct contact with the wall. The particular thickness does not matter as long as it is small enough to maintain a linear temperature profile.

The prescribed heat leak into the tank is the same for all of the cases presented here and equal to $Q_t = 2.83$ W. This is accomplished by prescribing a uniform heat flux of 0.01 mW/cm^2 over the entire tank-wall surface.

Certain sections of the wall are designated as *cold fingers* and identified by the thick solid lines in Fig. 1. These are areas upon which different boundary conditions are applied in certain cases to achieve a cooling effect. This is done by either fixing their temperature or prescribing a negative outward-pointing heat-flux vector. Note that not all of the cold fingers are used at the same time. If a cold finger is being used, then its surface area is subtracted from the total tank-wall surface area when computing the heat flux so that the total heat input Q_t is always the same.

In certain cases, a liquid jet is used to mix and possibly cool the bulk liquid. The jet enters from the bottom of the tank and is directed toward the vapor region by prescribing an upward parabolic velocity profile at the jet inlet to the tank (with an average velocity of $u_j = 0.5$ cm/s), as indicated in Fig. 1a. The liquid exits the tank through an outlet opening surrounding the jet inlet. Thus, it is inherently implied that the liquid jet recirculates through a short cylindrical reservoir at the bottom of the tank. In this way, the volume

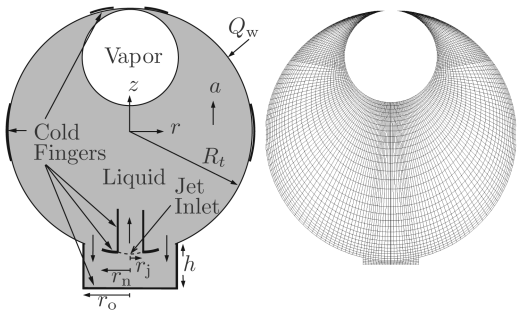

a) b)

Fig. 1 Illustrations of a) the geometry of the cryogenic tank model (not to scale) and b) a typical numerical mesh that is to scale. The vapor region is assumed to be spherical and stationary at one end of the tank.

of liquid cryogen in the tank is kept constant. If the jet is subcooled, then the desired subcooled temperature is prescribed at the jet inlet. Otherwise, the temperature at the inlet is left unspecified and the jet is used solely for mixing the bulk liquid. The standard no-slip velocity boundary condition is applied on all of the solid surfaces. The tank is completely closed and there is no flow into or out of the tank except for the jet flow.

The fluid flow and temperature distributions in the liquid region are determined by using an in-house customized version of the commercial finite element code FIDAP, as described by Panzarella et al. [27]. A typical mesh consisting of about 3451 9-node quadratic elements is shown in Fig. 1b. The mesh is modified for each case by locally refining it in regions with steep solution gradients, which usually arise near the walls, next to the cold finger, and at the liquid–vapor interface. At each time step, an iterative solution strategy is employed to solve the resulting matrix equations with a relative convergence tolerance of 10^{-6}. Time steps are chosen adaptively [28] to keep an estimate of the time truncation error less than 10^{-5}. Detailed numerical convergence studies for a similar model were conducted previously [3].

A lumped thermodynamic treatment of the vapor region is used to derive an approximate relationship for predicting the evolution of the tank pressure by invoking integral energy and mass balances over the vapor region. The details of this approach can be found elsewhere [3], but the primary assumptions that make such an analysis possible are that the vapor behaves as an ideal gas (for convenience, not a requirement) and that its pressure and temperature are nearly uniform. The temperature of the vapor at the liquid–vapor interface is assumed to be equal to the equilibrium saturation temperature corresponding to the total pressure. In addition, the kinetic energy, gravitational potential energy, and viscous dissipation contributions are all neglected with respect to the internal energy. If these assumptions hold, then to a good approximation, the integral balances of energy and mass simplify considerably and can be combined into a single nonlinear evolution equation for the average (denoted by an overbar) vapor pressure as follows:

$$\frac{\mathrm{d}\bar{p}_v}{\mathrm{d}t} = F(\bar{p}_v)Q_l \tag{1}$$

where Q_l is the net heat entering the vapor region through the liquid–vapor interface and F is a nonlinear function of vapor pressure given by

$$F(\bar{p}_v) = \frac{L}{V_v}\left\{c_v T_s + \left(\frac{Lm}{R_g T_s} - 1\right)\frac{\rho_l}{\rho_l - \rho_s} \cdot \left[L - \bar{p}_v\left(\frac{1}{\rho_s} - \frac{1}{\rho_l}\right)\right]\right\}^{-1} \tag{2}$$

The saturation temperature is related to the pressure through the Clausius–Clapeyron equation,

$$T_s(\bar{p}_v) = \left(\frac{1}{T_b} - \frac{R_g}{Lm}\ln\frac{\bar{p}_v}{p_b}\right)^{-1} \tag{3}$$

and the saturated vapor density is determined from the ideal-gas equation of state:

$$\rho_s = \frac{\bar{p}_v m}{R_g T_s} \tag{4}$$

Equation (2) is coupled to the governing equations in the liquid region through the heat flow term Q_l that is obtained by integrating the liquid-side heat flux over the entire liquid–vapor interface. Moreover, the liquid energy equation is coupled to Eq. (2) via the Clausius–Clapeyron equation through the imposition of the saturation temperature as the temperature boundary condition at the liquid–vapor interface. Thus, as the vapor pressure changes, so does the interfacial temperature, which directly affects the temperature field in the liquid and indirectly affects the flowfield through the temperature-dependent buoyancy term. This results in a modified interfacial heat flux that drives the pressure rise.

The most questionable assumption of the lumped-vapor approximation is that the temperature distribution in the vapor region remains nearly uniform. This assumption can be justified quantitatively for situations in which diffusive effects dominate by ensuring that $|Bi| \ll 1$, where $Bi = q_v R_v / k_v T_s$ is the generalized Biot number, R_v is the radius of the spherical vapor region, and q_v is a representative heat flux on the vapor side of the interface. The value of q_v can be estimated by assuming that it is equal to the total amount of heat required to raise the temperature of the vapor region (with total mass $\rho_v 4\pi R_v^3/3$) at the rate $\mathrm{d}T_s/\mathrm{d}t$, distributed uniformly across its surface area $4\pi R_v^2$:

$$q_v \approx \frac{1}{3} R_v \rho_v c_v \frac{\mathrm{d}T_s}{\mathrm{d}t} \tag{5}$$

This condition can then be checked once $\mathrm{d}T_s/\mathrm{d}t$ is computed for each case to ensure a consistent solution.

The previous condition assumes a quasi-steady balance between diffusion and the heat input through the vapor boundary. For this assumption to hold, the timescale associated with the changing saturation temperature must be much larger than the diffusive timescale $t_d = R_v^2/\alpha_v$:

$$\left|\frac{1}{T_s}\frac{\mathrm{d}T_s}{\mathrm{d}t}\frac{R_v^2}{\alpha_v}\right| \ll 1 \tag{6}$$

In other words, the saturation temperature must vary slowly enough so that diffusion has sufficient time to equalize the temperatures within the vapor region.

When the liquid mixing jet is used, convective effects dominate over diffusive effects and the vapor temperature will be mostly uniform, except possibly near the interface, where thin thermal boundary layers may develop in cases of rapid cooling. This can be seen by comparing the convective timescale defined by $t_c = R_v/u_j$ with the diffusive timescale $t_d = R_v^2/\alpha_v$. By using the parameter values listed in Table 1, $t_c \approx 110$ s, which is much less than the diffusive timescale $t_d \approx 1.2 \times 10^5$ s. Consequently, the vapor temperature away from the boundary will be nearly uniform. By equating the dominant diffusive and convective terms in the vapor

Table 1 Material properties of hydrogen and other parameters at the normal boiling-point temperature (20.39 K).

Parameter	Value
α_v, cm^2/s	0.0256
c_v, erg/K · g	1.012×10^8
k_v, erg/cm · s · K	4885
ρ_v, g/cm^3	0.00133
μ_v, g/cm · s	3.207×10^{-5}
L, erg/g	4.456×10^9
m, g/mol	2.0
h, cm	5
r_j, cm	15
r_o, cm	33
R_v, cm	55.26
T_b, K	20.27
T_j, K	20
β_l, 1/K	0.017
c_l, erg/K · g	9.7×10^7
k_l, erg/cm · s · K	12,440
ρ_l, g/cm^3	0.07047
μ_l, g/cm · s	1.327×10^{-4}
σ, dyn/cm	1.93
a, cm/s^2	981×10^{-6}
Q_l, W	2.83
r_n, cm	21
R_t, cm	150
R_g, erg/K · mol	8.31×10^7
p_b, atm	1.0
u_j, cm/s	0.5

energy equation, the boundary-layer thickness is found to be on the order of

$$\delta \sim \sqrt{\frac{t_c}{t_d}} = \sqrt{\frac{\alpha_v}{R_v u_j}} = 0.03 \text{ cm}$$

for the present case. To estimate the extent of the temperature jump across this boundary layer, we can assume that δ is the more appropriate characteristic length scale to use in the definition of the Biot number (i.e., $Bi_\delta = q_v \delta / k_v T_s$). Then, for the temperature jump across the boundary layer to be small, $|Bi_\delta| \ll 1$ as before. Again, this condition will be checked later for each case once $\mathrm{d}T_s/\mathrm{d}t$ has been computed so that q_v can be estimated.

As before, for this quasi-steady balance to hold, the saturation temperature must vary slowly when compared with the convective timescale:

$$\left| \frac{1}{T_s} \frac{\mathrm{d}T_s}{\mathrm{d}t} \frac{R_v}{u_j} \right| \ll 1 \tag{7}$$

This is another condition that will be checked once $\mathrm{d}T_s/\mathrm{d}t$ has been computed for those liquid-jet cases in which convective effects dominate.

The computation time for the results presented in the next section ranged from about 14 to 67 h (depending on the specific case) on a 1.6 GHz Intel Xeon-based Linux server with 16 GB of memory. Additional details on this approach and studies investigating the spatial and temporal convergence criteria have been previously reported in [3,27].

III. Results and Discussion

The cases presented here are for a 3-m-diam spherical tank, 95% full of liquid hydrogen, with the spatial configuration shown in Fig. 1. The tank is assumed to be in microgravity, and so the residual tank acceleration is assumed to be $a = 981 \times 10^{-6}$ cm/s^2, aligned with the symmetry axis for convenience. The thermophysical properties of hydrogen and other important geometric parameters are listed in Table 1.

Each case is started from an initial state of self-pressurization lasting 75 days, during which the tank is subject to a total constant heat input of $Q = 2.83$ W with all cooling mechanisms turned off. At the beginning of the pressurization stage, the tank is at an initial uniform temperature of 20 K, with a corresponding saturation pressure of 0.9032 atm. After the 75 days of self-pressurization the vapor pressure has risen to 1.513 atm with a corresponding saturation temperature of 22.13 K, as shown in Fig. 2a. Naturally, the liquid is thermally stratified in the pressurized state, and the maximum subcooling and superheat in the liquid due to this stratification are 0.28 and 0.14 K, respectively. The corresponding isotherm and streamline contours in the pressurized liquid at this time are shown in Fig. 2c. These contours have been combined into a single image with isotherms on the left half and streamlines on the right half of the tank to save space by exploiting symmetry. This is also done for the remaining temperature and streamline contour plots shown in this paper. There are always 10 isotherms and streamlines shown for each case, and they are evenly spaced between the minimum and maximum values.

The thermal stratification is influenced to some degree by mixing due to natural convection that is brought on by the residual acceleration. It might seem surprising to have such significant natural convection in microgravity unless you consider that the modified Grashof number (defined here in terms of the wall heat flux q_w as $Gr = a\rho_l^2 \beta_l q_w R_t^4 / k_l \mu_l^2$) scales to the fourth power of the tank radius. Thus, a large tank in microgravity can stratify like a small tank on the ground, although, of course, it would take much longer to reach the stratified state in microgravity. Also, the shape and position of the ullage in the two cases would be considerably different. For the case considered here, $Gr = 1.9 \times 10^7$, which is in the regime of laminar natural convection, and the maximum flow speed due to natural convection is 0.00313 cm/s, which is still very small. As mentioned,

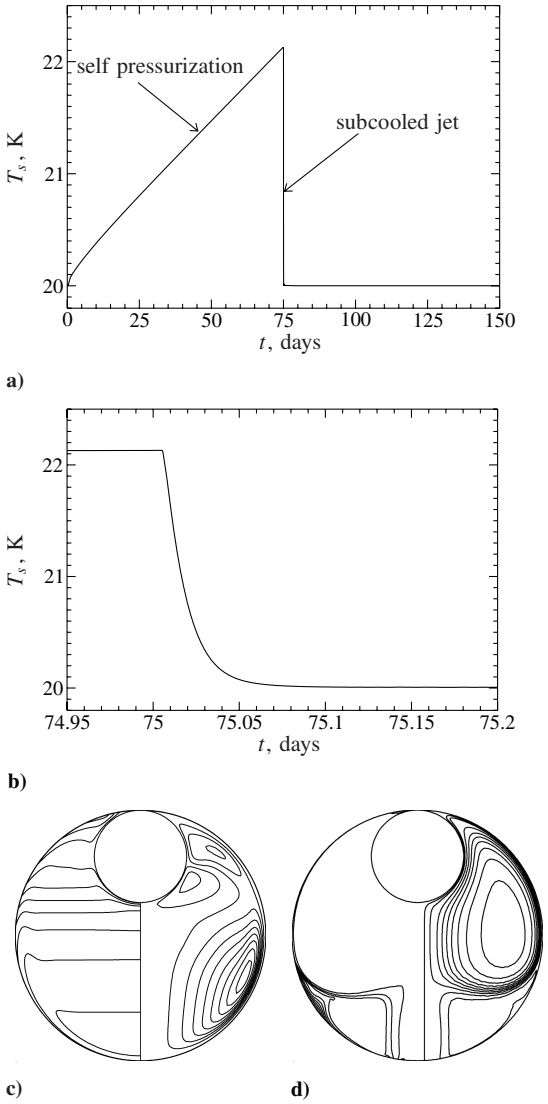

Fig. 2 The self-pressurization of a spherical cryogenic storage tank and subsequent cooling by a subcooled liquid jet turned on after 75 days. Effect on saturation temperature a) over the entire duration of the simulation and b) right after the jet is turned on, and 10 equally spaced isotherms/streamlines c) at 75 days ($T_{\min} = 21.85$ K, $T_{\max} = 22.27$ K, and $u_{\max} = 0.00313$ cm/s) and d) at 150 days ($T_{\min} = 20$ K, $T_{\max} = 20.13$ K, and $u_{\max} = 1.0$ cm/s). The contours are evenly spaced between the minimum and maximum values.

this final stationary state at 75 days is used as the initial condition for all of the subsequent cases presented here. A more detailed discussion of these numerical solutions can be found in our previous work [27].

Because

$$\frac{\mathrm{d}T_s}{\mathrm{d}t} \approx 3.3 \times 10^{-7} \text{ K/s}$$

for this case, $q_v \approx 0.82$ erg/cm$^2 \cdot$ s according to Eq. (5) and $Bi = 4.6 \times 10^{-4} \ll 1$. In addition, the condition given by Eq. (6) is also satisfied because

$$\frac{\mathrm{d}T_s}{\mathrm{d}t} \frac{R_v^2}{\alpha_v T_s} \approx 2 \times 10^{-3} \ll 1$$

Thus, this solution is consistent with the assumption of a nearly uniform temperature distribution in the vapor.

A. Subcooled-Liquid-Jet Mixing

Starting from the spatially stationary state resulting from 75 days of self-pressurization, as depicted in Fig. 2c, the subcooled liquid jet is turned on to quickly bring the ullage pressure and tank temperature back down to their initial unpressurized values, as also shown in Fig. 2. The prescribed temperature is 20 K at the jet inlet, the same as the initial tank temperature before pressurization. The jet is assumed to have a parabolic velocity profile with an average speed of 0.5 cm/s. As indicated by the rapidly dropping pressure and temperature curves in Fig. 2, this jet is capable of restoring the system to its initial state in about 2.5 h. The jet is kept on for a total of 75 days, but not much changes after the first few hours. Thus, in about 2.5 h, the jet effectively removes most of the heat that had accumulated during the prior self-pressurization interval of 75 days. Consequently, the average rate of cooling by the jet during this 2.5 h period is much larger than the rate of the constant heat leak into the tank.

Because the bottom of the ullage is about 190 cm away from the jet inlet, an overly simplistic calculation based on the amount of time it would take the jet, moving at an average jet speed of 0.5 cm/s, to cross this distance would predict the jet reaching the interface after only 380 s. It actually takes slightly longer, around 430 s, because buoyancy effects still play a role. Because the jet fluid is much colder than the surrounding liquid, it must overcome an additional buoyancy force that resists its upward motion. After about 15 min, the flow of jet fluid completely encapsulates the vapor region. Despite this, it still takes another 2 h before the ullage pressure returns to its initial value, because as the jet fluid moves around the vapor region it still absorbs a significant amount of heat from the surrounding warmer liquid. As a result, the jet must remove most of the heat from the surrounding liquid before significant ullage pressure reduction can be achieved.

Another way of looking at this is to compare the jet-cooling time to the amount of time required to recirculate the entire volume of liquid in the tank through the jet. Because the volumetric flow rate of the jet is 21.2 liter/ min and the entire volume of the liquid in the tank is 13,430 liters, it will take the jet about 10.6 h to recirculate this entire volume. Although this value is comparable with the time it takes the jet to reduce the pressure to its initial value, it is still about 4 times longer, indicating that by directing the jet toward the vapor region, a more rapid pressure control can be achieved.

The final saturation temperature at 150 days is $T_s = 20.00017$ K. The final maximum subcooling and superheat in the liquid are 1.7×10^{-4} and 0.13 K, respectively. The subcooling is small because the cold jet fluid effectively encapsulates the entire vapor region. The superheat is still comparatively large because the cooler jet fluid moves around a stagnation region near the bottom tank wall. This shows that even with a jet, some parts of the tank are cooled better than others, depending on the particular flow pattern. Therefore, it is very important to direct the jet at the vapor region to achieve the most effective pressure drop. These considerations can become quite important and more complex if flow-management baffles are implemented in the tank.

It seems somewhat inefficient and unnecessary to run the subcooled jet continuously, because most of the cooling was achieved within a very short period of time. Thus, an intermittent jet flow strategy can be adopted. For example, it was just shown that by keeping a 0.5 cm/s subcooled jet on for 2.5 h, it is possible to remove all of the internal energy that has accumulated over the initial 75 days of self-pressurization, thus returning the tank quite rapidly to its initial state. At this point, the jet could be turned off for another 75 days of self-pressurization, followed by another 2.5 h jet-cooling period. This cycle of self-pressurization and intermittent subcooled-jet cooling could be repeated over and over again, as many times as required. The saturation temperature would cycle back and forth between the values 20 and 22.13 K, and the pressure would cycle between 0.9032 and 1.513 atm. Of course, for each specific application, the intermittency cycle and jet parameters must be optimized so that the temperature and pressure will not rise beyond their intended design specifications and margin of safety. Furthermore, the jet speed can easily be increased to achieve pressure-reduction times that are 10–20 times shorter.

The saturation temperature decreases very rapidly in this case because the subcooled liquid jet is very effective. Specifically, the largest value of $|\mathrm{d}T_s/\mathrm{d}t|$ is

$$\left|\frac{\mathrm{d}T_s}{\mathrm{d}t}\right| \approx 8 \times 10^{-4} \text{ K/s}$$

from which it follows that $q_v \approx 2 \times 10^3$ erg/cm$^2 \cdot$ s according to Eq. (5). Despite the rapid cooling rate, $Bi_\delta \approx 6 \times 10^{-4} \ll 1$ for this case. In addition, the condition given by Eq. (7) is also satisfied because

$$\frac{\mathrm{d}T_s}{\mathrm{d}t}\,\frac{R_v}{u_j T_s} \approx 4.4 \times 10^{-3} \ll 1$$

Thus, this solution is also consistent with the assumption of a nearly uniform temperature distribution in the vapor, even though the saturation temperature is rapidly decreasing. Because this case exhibits the most rapid cooling rate, these conditions will not be explicitly checked for the remaining cases because they will undoubtedly hold.

B. Cold-Finger Cooling with Separate Jet Mixing

Although the subcooled jet is perhaps the most rapid and effective method of reducing the pressure, it may not be efficient to keep the pump-driven jet working continuously. It may prove worthwhile to separate the cooling and mixing operations so that, for example, the cooling can be done continuously while the pump is turned on and off to provide intermittent mixing. This can be accomplished through a cold finger and an uncooled mixing jet that operate independently of each other.

In this context, the next series of case studies use an uncooled mixing jet along with a separate cold finger that is placed at different locations along the tank wall. The effect of the cold finger is simulated by fixing the temperature of a specific section of the tank wall to the initial subcooled temperature of 20 K. To make a fair comparison, the net heat input is kept the same as before by increasing the prescribed heat flux on the remaining "uncooled" surface area. The initial condition for all of these cases is the same as before, and the stationary state is achieved after 75 days of initial self-pressurization. The characteristics of the jet are also the same as before, except that its temperature is no longer controlled. Hence, it provides mixing without any active cooling.

In the first case, the cold finger is placed on a section of the tank sidewall between -30 cm $< z < 0$. As shown in Fig. 3a, this approach results in a significantly less effective pressure control than with the subcooled jet, because it now takes over a month to get a comparable reduction in pressure and temperature. Even then, the final saturation temperature (20.0813 K) is much further from its initial value than before. However, it must be noted that once the temperature reaches this level, the cold finger is capable of maintaining this temperature level for a long period of time. Thus, for long-duration storage, if rapid pressure control is not required, this strategy may be acceptable for limiting the pressure rise.

It must also be kept in mind that this case is less effective because the rate of cooling is limited by how fast heat can be removed from the liquid as the jet fluid passes over the cold finger, and a flat plate with no fins is a rather inefficient heat exchanger. Thus, the performance of this approach can be improved through several engineering design considerations such as adding fins to increase the surface area of the cold finger, lowering the temperature of the cold finger, or increasing the jet speed, all of which are outside the scope of the present paper.

It is also interesting to note the very early behavior of the saturation temperature, as shown in Fig. 3b. For the first couple of hours, the temperature drops rapidly as the jet destratifies the liquid by mixing the cooler fluid from the bottom of the tank with the slightly warmer liquid closer to the vapor region. Of course, this cooling effect is not the result of any active cooling by the cold finger but is merely due to the disruption of thermal stratification that had already been established by natural convection. However, once the jet passes around the vapor region, it heats back up as it is deflected from the

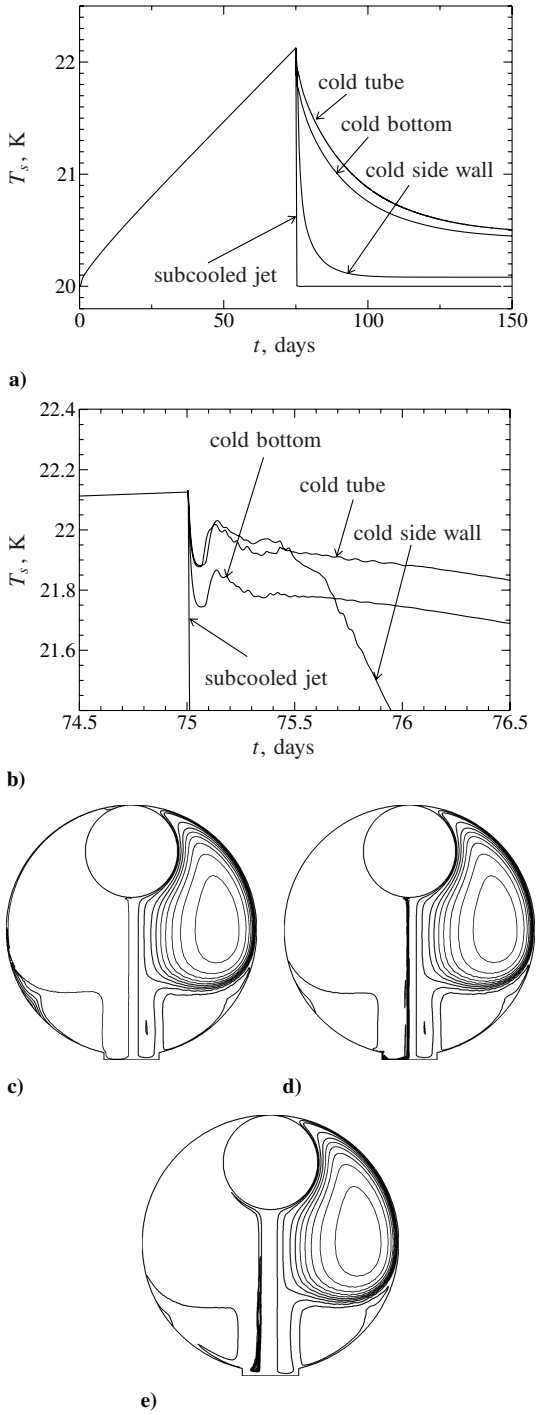

Fig. 3 Cooling with separate jet mixing effect on a) long-term saturation temperature, b) short-term saturation temperature, and the 10 equally spaced isotherms/streamlines after 150 days for the c) cold finger on side wall ($T_{min} = 20$ K, $T_{max} = 20.18$ K, and $u_{max} = 1.0$ cm/s), d) cold finger at the bottom ($T_{min} = 20$ K, $T_{max} = 20.59$ K, and $u_{max} = 1.0$ cm/s), and e) cold tube surrounding the jet ($T_{min} = 20$ K, $T_{max} = 20.62$ K, and $u_{max} = 1.0$ cm/s).

warmer tank wall, then it turns around and carries that warmer liquid back toward the vapor region in a recirculating motion. This leads to subsequent temperature and pressure rise for the next couple of hours.

Our simulations indicate that the thermal state of the tank is unaffected by the presence of the cold finger for the first 5 h (further verified later) and is primarily influenced by the disruption of the thermal stratification brought about by the jet. Eventually, after about 0.5 days, the slowly expanding path of the recirculating jet fluid finally reaches the cold finger at the side wall, and as a result, colder fluid is carried on to the area closer to the vapor region. This initiates a slow but steady drop in temperature and pressure that continues from that point on.

Note from the final isotherms and streamlines shown in Fig. 3c that the temperature distribution in the liquid is nearly uniform almost everywhere except for near the cold finger and directly beneath it, where there is a hot spot on the tank wall. This hot spot is again due to a stagnant region near the tank wall in which the cooler jet fluid is unable to penetrate, as indicated by the associated streamline plot. The final maximum subcooling and superheat in the tank for this case are 0.081 and 0.10 K, respectively.

The subcooling is larger here than in the subcooled-jet case because the cooling is separated from the mixing. The jet fluid has to pass over the cooler section of the tank wall and travel through the bottom of the tank and upward along the centerline before reaching the ullage. It heats up along this path so that it is much warmer by the time it reaches the vapor. The superheat is slightly lower than before because the cold finger is closer to the stagnation region in which the hot spot is located.

In the next case, the cold finger is moved to the bottom of the tank by prescribing a temperature of 20 K on the walls enclosing the cylindrical reservoir beneath the jet inlet. From the resulting saturation temperature curve shown in Fig. 3a (cold-bottom case), it is immediately clear that this approach is even worse than the previous case because the saturation temperature is decreasing at a much slower rate. It does not even reach a steady state within 75 days. This is primarily due to a reduction in the cold-finger surface area, which is now only about 16% of what it was in the previous case. Basically, this reduction in surface area leads to a slower cooling rate for the same jet speed. Again, this just shows that the cold finger in this case is acting like an inefficient heat exchanger because it is essentially a smooth, flat surface. There is no doubt that adding fins to increase the heat exchange surface area would noticeably increase the efficiency of this process. In the limit of an ideal heat exchanger, this case should have a performance identical to the subcooled-jet case. However, it would be quite difficult to approach the ideal heat exchanger merely through the placement of fins on the cold finger.

Given enough time, even this case will eventually approach a steady state in which the net cooling rate exactly balances the rate of heat input, but to achieve this with a lower cold-finger surface area and a jet speed of 0.5 cm/s, the temperature of the cold finger must be significantly reduced.

The final isotherms and streamlines for this case are shown in Fig. 3d. The final maximum subcooling and superheat are 0.45 and 0.14 K, respectively. The subcooling is much larger for the reason just mentioned (to maintain the same steady-state cooling rate with a low cold-finger surface area), but the superheat is still about the same because the stagnation region is mostly unaffected by this change.

Note from Fig. 3b that the oscillation of the saturation temperature over the first 5 h or so is similar to the previous case, except that the curve is shifted down by some fixed amount. As before, this is still characteristic of the disruption of thermal stratification, but with an additional modest cooling effect due to the cold finger.

The final case of this series consists of a cold finger that is a 40-cm-long cylindrical tube surrounding the jet inlet, as illustrated in Fig. 1. The tube is at a prescribed temperature of 20 K along its entire length. The surface area of this tube is about the same as the surface area of the cold finger in the previous case, and so, as expected, the overall cooling rate is about the same as before, as shown in Fig. 3a. This reinforces the notion that the average long-term cooling rate is roughly proportional to the surface area of the cold finger if the temperature and flow speed are the same. Undoubtedly, the heat transfer in this case could be greatly enhanced by adding a series of radial fins to the interior of the tube, but this would also come at the expense of disrupting the jet flow. Again, in the limit of an ideal heat exchanger, this case should perform almost equally as well as in the subcooled-jet case.

The final isotherms and streamlines for this case are shown in Fig. 3e. The final maximum subcooling and superheat are 0.51 and 0.11 K, respectively. Note that the subcooling is about the same as in the previous case. Again, the larger subcooling is an indication of a

less efficient cold finger, because a larger temperature drop is required to achieve the same steady-state cooling rate. Finally, the results of these cases seem to indicate that the efficiency of the cold finger depends very much on its surface area, but not as much on its particular geometry or location within the tank.

C. Cold-Finger Cooling Without Forced Mixing

The previous cases have shown that even with forced mixing, the overall pressure-reduction capability is greatly reduced when the mixing and cooling elements are separated. In this section, we will examine the case in which there is active cooling without any forced mixing, although there can still be some mixing due to natural convection brought about by the residual acceleration. This strategy is advantageous because it is simpler, requires less power, and is less susceptible to mechanical failure associated with the operation of the pump. Also, if the pump used for forced mixing were to fail, then the tank is subject precisely to such a situation in which cooling by the cold finger is not accompanied by any active mixing. As a result, this scenario also needs to be understood and studied from a risk-mitigation point of view.

In the first case examined here, the cold-finger configuration is the same as in the first case of the previous section (along the middle section of the tank wall). Again, the temperature of the cold finger is immediately dropped to 20 K after 75 days of self-pressurization, but now there is no jet, and the only mixing in the liquid is due to natural convection.

For the first 5 days or so, the saturation temperature continues to rise, but at a slowly decreasing rate, as shown in Fig. 4a. During this time, the temperature field exhibits numerous small-scale oscillations, as shown in Fig. 4b, due to the complex flow patterns arising from natural convection. Beyond the first week, the temperature levels finally start to slowly decrease. By the 75th day, the ullage temperature appears to plateau, but to a level that is still much greater than its initial value of 20 K. This is not surprising, because without any forced mixing, heat is transferred primarily by conduction alone. The final maximum flow speed due to natural convection is only 0.00585 cm/s. This provides much less mixing than the forced jet at an average speed of 0.5 cm/s.

The final isotherms and streamlines for this case are shown in Fig. 4c. It is clear that the fluid above the cold finger is relatively stagnant, even though it exhibits some signs of thermal stratification due to natural convection, whereas the fluid below the cold finger appears to be well mixed and nearly isothermal. This is because the cooler fluid near the cold finger tends to sink to the bottom of the tank, leading to vigorous mixing and resulting in a nearly constant temperature region. The warmer liquid above the cold finger is in a more thermally stable configuration with respect to the colder fluid beneath it, which explains why the region above the cold finger is relatively stagnant. The final maximum subcooling and superheat in this case are 1.28 and 0.20 K, respectively.

When steady state is achieved, the net cooling rate will still balance the rate of heat input, but because the heat is now primarily transported by conduction, this is accomplished by a larger temperature difference between the cold finger and bulk liquid. This is why the final subcooling is so large.

Finally, it is again noted that even though this approach is not capable of bringing the tank temperature back down to its initial value, it is still quite capable of preventing any further pressure rise, which may be an acceptable situation for long-duration storage in which rapid pressure control is not required.

Because the fluid beneath the cold finger is well mixed in the case just examined, it was thought that perhaps by raising the height of the cold finger, enhanced mixing of the entire liquid region could be achieved. This requires the cold finger to be placed closer to the vapor region, so that a more rapid response can be expected. The case is examined next in which the cold finger is positioned closer to the vapor region at the top of the tank, specifically covering the section of the upper tank wall lying between $r_n < r < r_o$, as shown in Fig. 1. Unfortunately, its surface area is only about 7.3% of that in the previous case, and so it is expected that its cooling effectiveness will

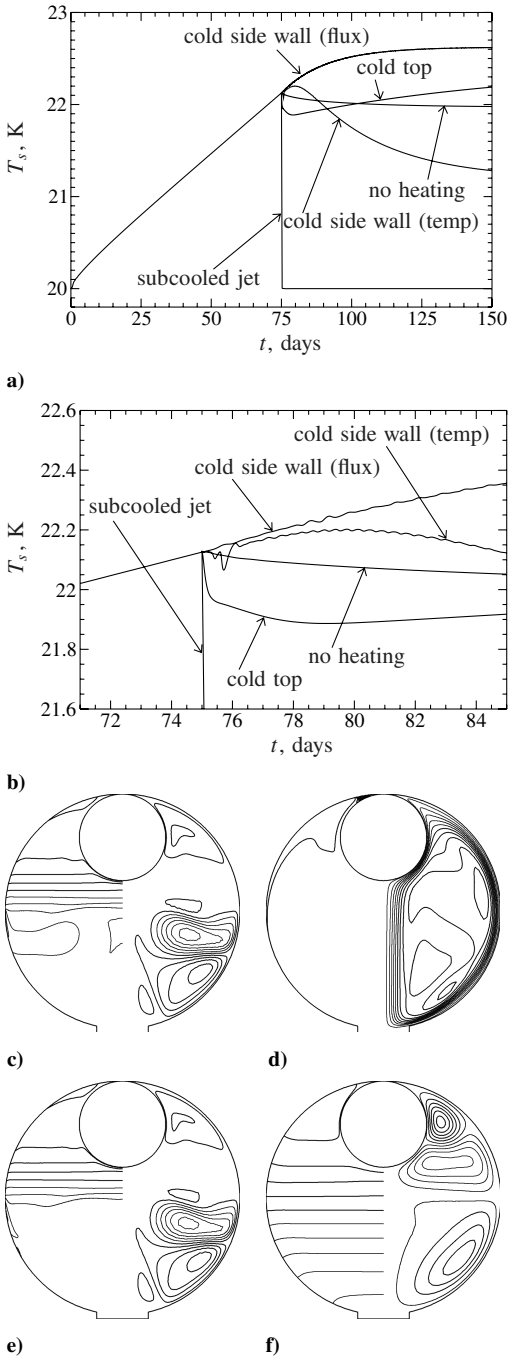

Fig. 4 Cooling without forced mixing effect on a) long-term and b) short-term saturation temperature, and 10 equally spaced isotherms/streamlines after 150 days for c) cold finger on side wall with fixed temperature ($T_{min} = 20$ K, $T_{max} = 21.48$ K, and $u_{max} = 0.00585$ cm/s), d) cold finger on top wall ($T_{min} = 20$ K, $T_{max} = 22.51$ K, and $u_{max} = 0.00986$ cm/s), e) cold finger on side wall with fixed heat flux ($T_{min} = 21.29$ K, $T_{max} = 22.81$ K, and $u_{max} = 0.00554$ cm/s), f) no heating ($T_{min} = 21.96$ K, $T_{max} = 21.98$ K, and $u_{max} = 2.34 \times 10^{-4}$ cm/s).

be reduced. As before, cooling is achieved by specifying the temperature of this cold finger to be 20 K after the 75 days of initial self-pressurization.

Figure 4b indicates that these changes do have the desired effect when implemented, but only for a while. The saturation temperature drops more rapidly for the first 5 h than in any other case without forced mixing, because the cold finger is much closer to the vapor region. Unfortunately, this is short-lived because the rate of decrease slows down significantly after a while, and after about 4 days, the saturation temperature starts rising again and continues to rise for the

next 75 days, as shown in Fig. 4a. The final saturation temperature after 150 days is actually slightly greater than the temperature before the cold finger was activated. A transition in slope occurring at around 5 h is due to a shift in the flow pattern from the three recirculation zones shown in Fig. 2c to just two primary zones. This is a consequence of the colder fluid falling down around the vapor region. The maximum flow speed after 5 h also increases to 0.00986 cm/s. This shift in the flow pattern brings in warmer fluid from the tank wall and slows down the cooling rate.

After about 4 days, the flow pattern makes another shift to one primary recirculation zone moving upward around the entire perimeter of the tank wall, engulfing the vapor region and then sinking straight down the centerline to the bottom of the tank, as shown in Fig. 4d. This flow is driven by the cooler fluid from the cold finger, which is heavier and therefore sinking due to reverse buoyancy. The reversal in the slope of the saturation temperature curve at this time is due to enhanced heat transfer from the warmer side walls due to this recirculation zone, which consequently leads to an increasing saturation temperature.

Overall, the liquid is well mixed in this case, as indicated by the isotherm plot shown in Fig. 4d except for liquid immediately adjacent to the cold finger that is relatively stagnant due to its close proximity to the obstructing vapor region. This, combined with the significant reduction in cold-finger surface area, results in a net cooling rate that is insufficient to counter the rate of heat leakage into the tank. As a result, the saturation temperature continues to rise.

The final maximum subcooling of 2.19 K occurs right at the location of the cold finger. It is rather large because the saturation temperature is still close to its initial value, due to the ineffectiveness of the cold finger in this case, whereas the temperature of the cold finger remains at its specified temperature of 20 K. The final maximum superheat is 0.32 K, which is larger than in any of the previous cases, because the liquid moving upward along the tank wall carries a significant amount of heat, resulting in a hot spot on the upper tank wall.

In the next case that is considered, a constant negative heat flux is prescribed on the surface of the cold finger, rather than a prescribed temperature. Thus, the rate of heat removal from the tank is now fixed, whereas before, it depended on the local temperature gradient at the cold-finger surface, as dictated by the neighboring flow pattern. The cold finger is again placed on the sidewall at the middle of the tank with the same location and surface area as in the corresponding prescribed temperature case previously discussed. The value of the heat flux is chosen so that total heat extracted by the cold finger exactly balances the 2.83 W leaking into the tank through the remaining wall surfaces. As a result, the net heat input into the tank is zero.

Even though the net heat input is zero, the saturation temperature continues to rise for the next 75 days, as shown in Fig. 4a. It does start leveling off near the end as it should, but only after a long period of time has elapsed. This case is significantly different from the fixed-temperature case, in which a much faster cooling rate was attained. This is due to the fact that when the temperature of the cold finger is fixed to 20 K, the initial rate of heat removal is 27.6 W, almost an order of magnitude larger than the heat removal prescribed on the cold finger in the present case. The final isotherms and streamlines for this case are shown in Fig. 4e. As before, the liquid below the cold finger is well mixed, but significant thermal stratification is observed above the cold finger. The final maximum subcooling and superheat are 1.33 and 0.19 K, respectively. The final maximum flow speed due to natural convection is 0.00554 cm/s.

It is interesting to compare the present case to one in which the heating is simply turned off by setting the heat flux to zero on all surfaces. Even though the net heat input is zero in both cases, the final steady-state solutions are quite different, as demonstrated through a comparison of the resulting saturation curves in Fig. 4a. When the heating is turned off completely, the temperature and pressure decrease slowly as thermal stratification slowly diminishes and the liquid and vapor regions become isothermal. Even after 75 days, an isothermal state has not yet been reached, due to the long timescales associated with conduction and natural convection. This can be seen in Fig. 4f, in which the maximum subcooling and superheat are still 0.018 and 0.00103 K, respectively. The maximum flow speed due to natural convection at this time is only 2.34×10^{-4} cm/s.

Even though the previous two cases both have a net heat input of zero, the final saturation temperatures are quite different because the temperature distributions in the liquid are different. In the previous case, in which the heat flux on the tank wall is set to zero everywhere, the liquid will eventually become isothermal. However, if the heat flux is positive on some surfaces and negative on others, temperature gradients will develop in the liquid between these surfaces, even if the net heat input is zero. Moreover, the saturation temperature and corresponding tank pressure can also be quite different, depending on the position of the ullage within this thermal gradient. These results clearly show that the distribution of heat in the liquid and the position of the ullage in the resulting thermal field are crucial factors that need to be considered.

Unfortunately, these differences are indistinguishable when using a purely thermodynamic model of the entire tank, because that would be solely based on the net heat input and does not take into account the different heat distributions caused by dynamic transport. Therefore, computational fluid dynamics simulations are necessary for predicting the dynamic response of tank pressure in space, especially because, for larger tanks in microgravity, the relative impact of these dynamic changes is much larger and persists longer than for smaller tanks on the ground.

In general, without some form of forced mixing, the cooling rate of a cold finger is inherently limited because, by itself, it is not a very effective heat exchanger. This has an important practical consequence: it is not always possible to control the rate at which heat is extracted by a cold finger. In other words, for any given geometrical configuration, there is an upper bound to the maximum possible cooling rate of a cold finger, because it can only remove heat as fast as it can be transported to it through the surrounding liquid, and this depends on the heat flux (temperature gradient) in the liquid immediately adjacent to its surface. For a system without forced mixing, heat is transported primarily by conduction, and the maximum heat flux is dictated by the temperature difference between the cold finger and the saturation temperature as well as the distance between them. This is a fundamental limitation that cannot be overcome without the use of some forced mixing. Thus, beyond a certain point, increasing the surface area of the cold finger alone cannot be the remedy.

For instance, because the cold finger can obviously never have a temperature less than 0 K, and the temperature of the cryogenic liquid is always going to be around its normal boiling-point temperature, which is nearly 20 K for liquid hydrogen, a good estimate of the maximum possible temperature difference in the liquid is $\Delta T = 20$ K. Using this characteristic temperature difference along with estimates of the average distance d between the cold finger and the vapor region and the total surface area A of the cold finger, the maximum possible cooling rate provided by an idealized cryocooler under near-stagnant conditions in the tank is approximately $Ak_l\Delta T/d$. If d is one-half of the tank radius and A is $1/10$ the total tank-wall surface area, then the maximum cooling rate for the cold finger is estimated to be at most 10 W for the present tank design. This is significantly less than the cooling rate of 2 kW provided by the subcooled jet.

Of course, this is only a rough estimate, and a better one could be obtained through more detailed numerical simulations such as those presented here. However, this does not alter the fact that if a large cooling rate is required, then some form of forced mixing must be implemented. Natural convection may increase the conduction-limited cooling rate somewhat, but not by much under microgravity conditions. As always, additional modest improvements can be made by increasing the surface area of the cold finger or by placing it closer to the vapor region.

D. Mixing Without Cooling

It is also interesting to see what effect mixing without any active cooling has on the temperature and pressure rise in the tank, and so

this case is considered next. Because of thermal stratification due to residual gravity, cooler liquid still sinks to the bottom of the tank and warmer liquid floats to the top in the absence of any forced mixing. Thus, as shown in Fig. 2c, there is a 0.42 K temperature difference established between liquid at the top and bottom of the tank before turning on the jet. Once the jet is turned on, this cooler fluid at the bottom can be brought up to the warmer vapor region, leading to a momentary cooling effect that is just due to mixing and thermal destratification.

This mixing/destratification effect is clearly shown in Fig. 5. At the onset of mixing, there is a momentary drop in the saturation temperature for about 2 h as the colder fluid from the bottom of the tank is brought into contact with the vapor region, but this is followed by a subsequent rise in temperature as the jet is deflected by the tank wall, starts recirculating, and eventually starts to carry warmer fluid around with it. Gradually, the oscillations settle down, and the rate of pressure and temperature rise return to normal, as they should according to thermodynamics, because the net heat input is still the same. The final isotherms and streamlines are shown in Fig. 5c. The maximum subcooling and superheat at that time are 0.16 and 0.080 K, respectively. These are smaller than before, due to the enhanced mixing effect provided by the jet.

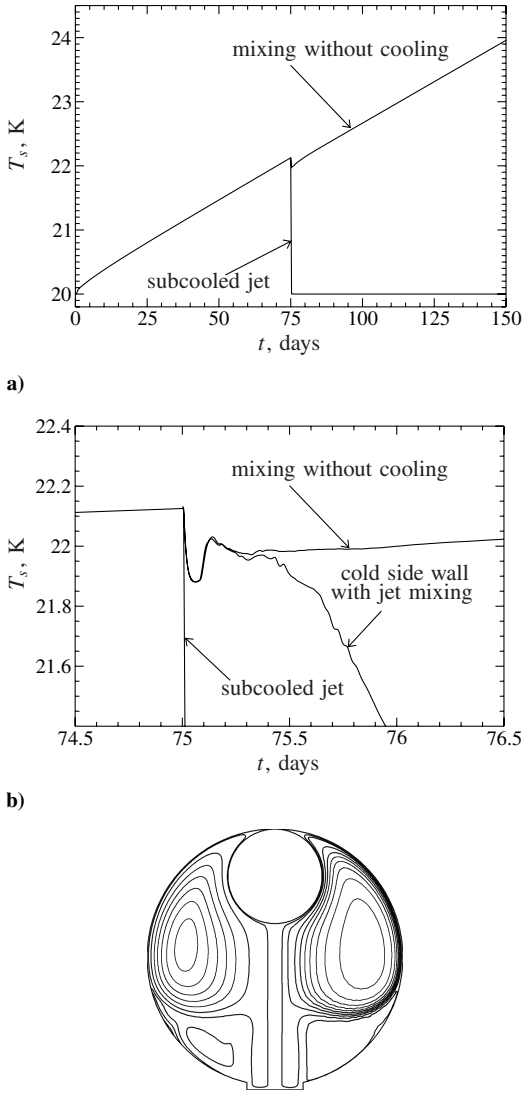

Fig. 5 Mixing without cooling. An uncooled liquid jet is used to mix the liquid and disrupt thermal stratification. Effect on a) long-term saturation temperature, b) short-term saturation temperature, c) 10 equally spaced isotherms/streamlines after 150 days ($T_{\min} = 23.80$ K, $T_{\max} = 24.04$ K, and $u_{\max} = 1.0$ cm/s).

Finally, it is interesting to note that for about the first 5 h, the response of the saturation temperature in the mixing-only case is nearly identical to that for the earlier case of an uncooled jet with a separate cold finger on the side wall, as shown in Fig. 5b. This further justifies the previous assertion that the early response in that cold-finger case is due to thermal destratification by the jet and has very little to do with the presence of the cold finger itself.

IV. Summary

It is clear from the results presented in the previous section that the most rapid and effective method of controlling the tank pressure is through a subcooled jet directed toward the ullage. In this case, the mixing and cooling mechanisms are simultaneously applied and integrated. Our numerical simulations indicate that it is possible to remove all of the internal energy accumulated during a self-pressurization period of 75 days in just over 2 h with a subcooled jet. No other approach considered here was found to be as effective at controlling the pressure. However, it is recognized that this is an ideal situation that may never be realized, because the vapor would likely not stay in one place under the action of the jet, but would rather be pushed to one side or another. A dynamic simulation taking into account the motion of the vapor region throughout the tank would be required to get a more accurate representation of what would actually happen in practice. The present results are useful because they represent a best-case scenario that can be strived for, even if never fully realized.

Of course, to achieve such rapid cooling, the subcooled jet has to remove heat at an average rate of about $Q_t(75 \text{ days}/0.1 \text{ days}) \approx 2$ kW during a short period of time. This implies that the jet must pass through a highly effective heat exchanger that is capable of maintaining the inlet jet temperature at 20 K. This is achieved in the model by simply prescribing the temperature of the jet fluid at the inlet, but in practice, a highly efficient heat exchanger would be needed for this purpose.

It does not seem necessary to operate the subcooled jet continuously once it has brought the tank pressure back down to its initial level. Therefore, it is suggested here that the jet be operated intermittently. For example, in a typical scenario such as that considered here, the jet can be used for 2.5 h to achieve the desired cooling effect and then turned off for an interval of up to 75 days, during which there is a period of self-pressurization, which can be followed by an additional cooling jet interval, and so on. Of course, the period of time between cooling events and the jet speed can be adjusted to provide faster or slower pressure-reduction rates to accommodate engineering and design tradeoffs and to account for changing environmental conditions.

In addition to the subcooled jet, three alternative pressure-reduction strategies were considered: 1) the simultaneous use of separate cooling and mixing mechanisms, 2) the use of cooling elements alone without any forced mixing, and 3) mixing alone without any active cooling. These alternatives are of interest for several reasons. First, the additional mechanical complexity and power requirements of a mixing jet may not be warranted or necessary in all circumstances. Second, from a reliability point of view, the jet or the cryocooler may not be operational due to mechanical failure, in which case the effectiveness of cooling alone or mixing alone must be assessed to develop proper risk-mitigation strategies. Finally, the thermal destratification brought about by mixing alone may prove to be sufficient for many short-duration pressure control requirements.

When an uncooled mixing jet is used along with a separate cold finger, the pressure can still be controlled, but much more slowly, over a period of days or months instead of hours. The steady-state ullage temperature will also not be as close to the cold-finger temperature as in the subcooled-jet case. The effectiveness of this approach depends very much on the volume of liquid transported over the cold finger by the jet as well as the cold finger's ability to extract heat from that liquid. No attempt was made to optimize the heat transfer characteristics of the cold finger in this paper, but it was clearly established that faster cooling rates are obtained if the cold

finger's effective surface area is increased. Cold fingers with different geometries and locations but with similar surface areas yielded similar cooling rates.

Essentially, the cold finger has to be designed as an efficient heat exchanger, but from a volume-to-surface-area perspective, it is much more difficult to achieve high heat transfer efficiency with a stationary cold finger inside the tank than with an external heat exchanger used in conjunction with a forced liquid jet, as demonstrated in this paper.

A cold finger was also used without any forced mixing. This proved to be somewhat effective at limiting further pressure rise, but not that effective at removing the stored internal energy that had accumulated during the initial period of self-pressurization. Again, the cold finger was found to be slightly more effective if it had a larger effective surface area.

Although this paper only considered steady accelerations, it is interesting to consider what effect other types of accelerations such as vibrations, thruster firings, and changes in orientation might have on these results. It is unlikely that high-frequency vibrations would have any significant effect, because the timescale of those vibrations would normally be much less than the long diffusive and natural convective timescales observed here, and so they would just likely average out. Only the average acceleration over these longer timescales would be of any significance.

Panzarella and Kassemi [26] showed that the initial pressurization rate is quite different, depending on whether the vapor region is in the center of the tank or near the wall as it is here. If the vapor is near the wall, then it experiences a more rapid pressure rise and can respond more quickly to changes in external heat inputs because it takes less time for the heat to reach it. If it is in the center of the tank, the heat must diffuse through more liquid before reaching the vapor, and so it takes longer for the effect of any external change to be observed. It was also shown that it only takes about 10 min for a vapor region starting at the center of tank to reach the tank wall with the steady average acceleration considered here.

Thus, in the event of a thruster acceleration or change in orientation of any significant duration, the vapor region would likely drift from one location to another, and because of the lengthy diffusive and natural convective timescales, there would be significant oscillations in the pressurization rate, and it would take days for the tank to settle back down into the quasi-steady state observed here. Because the subcooled liquid jet was found to be the most effective at rapidly controlling the pressurization rate, it could be used during such an event, if necessary, to provide a more rapid response rate. Because the timescale of the jet is very short and its effect overwhelms that of natural convection, it is unlikely that the results for that case would depend significantly on the acceleration level.

V. Conclusions

This paper presents an in-depth comparative analysis of several different mixing/cooling strategies for ZBO tank pressure control in microgravity. The analysis was based on numerical simulations generated by a novel two-phase flow model that tightly couples a lumped thermodynamic treatment of pressure evolution in the vapor ullage to the direct numerical solution of the Navier–Stokes and energy equations in the liquid.

From our numerical results it can be concluded that for the most rapid and precise pressure control of large cryogenic storage tanks, a subcooled jet directed at the ullage is seemingly the best choice among the different strategies examined here. For long-duration storage in which it is more important to simply limit the pressure rise rather than control it or bring it down, the cooling and mixing mechanisms can be separated, and even cooling alone without any forced mixing can be considered, because it still benefits to a degree from limited mixing brought about by natural convection due to the residual buoyancy force. Finally, mixing alone without cooling can only provide limited pressure management through thermal destratification in very short-term applications.

This paper did not consider optimizing the direction of the jet flow for the specific cold-finger operations. It also did not present an in-depth quantitative analysis of the effects of the cold finger and jet temperatures or the effective surface area of the cold finger. A comprehensive examination of these important parameters will be presented in future work.

Acknowledgments

This work has been supported by the Cryogenic Fluid Management (CFM) project under NASA's Exploration Technology Development Program. The valuable technical discussions and suggestions provided by David Plachta, David Chato, and Jeffery Moder at NASA John H. Glenn Research Center at Lewis Field are also gratefully acknowledged.

References

[1] Salerno, L. J., and Kittel, P., "Cryogenics and the Human Exploration of Mars," *Cryogenics*, Vol. 39, No. 4, 1999, pp. 381–388. doi:10.1016/S0011-2275(99)00043-0

[2] Kittel, P., and Plachta, D. W., "Propellant Preservation for Mars Missions," *Advances in Cryogenic Engineering*, Plenum, New York, Vol. 45, 2000, pp. 443–450.

[3] Panzarella, C. H., and Kassemi, M., "On the Validity of Purely Thermodynamic Descriptions of Two- Phase Cryogenic Fluid Storage," *Journal of Fluid Mechanics*, Vol. 484, June 2003, pp. 41–68. doi:10.1017/S0022112003004002

[4] Aydelott, J. C., "Effect of Gravity on Self-Pressurization of Spherical Liquid-Hydrogen Tankage," NASA TN-D-4286, Dec. 1967.

[5] Aydelott, J. C., "Axial Jet Mixing of Ethanol in Cylindrical Containers During Weightlessness," NASA TP-1487, July 1979.

[6] Aydelott, J. C., "Modeling of Space Vehicle Propellant Mixing," NASA TP-2107, Jan. 1983.

[7] Lin, C. S., Hasan, M. M., and Van Dresar, N. T., "Experimental Investigation of Jet-Induced Mixing of a Large Liquid Hydrogen Storage Tank," AIAA Paper 94-2079, July 1994.

[8] Poth, L. J., and Van Hook, J. R., "Control of the Thermodynamic State of Space-Stored Cryogens by Jet Mixing," *Journal of Spacecraft and Rockets*, Vol. 9, No. 5, 1972, pp. 332–336.

[9] Cha, Y. S., Neiman, R. C., and Hull, J. R., "Thermodynamic Analysis of Helium Boil-Off Experiments with Pressure Variations," *Cryogenics*, Vol. 33, No. 7, 1993, pp. 675–679. doi:10.1016/0011-2275(93)90018-J

[10] Vaughan, D. A., and Schmidt, G. R., "Analytical Modeling of No-Vent Fill Process," *Journal of Spacecraft and Rockets*, Vol. 28, No. 5, 1991, pp. 574–579.

[11] Lin, C. S., and Hasan, M. M., "Self Pressurization of a Spherical Liquid Hydrogen Storage Tank in a Microgravity Environment," AIAA Paper 92-0363, Jan. 1992.

[12] Hochstein, J. I., Gerhart, P. M., and Aydelott, J. C., "Computational Modeling of Jet Induced Mixing of Cryogenic Propellants in Low-g," AIAA Paper 84-1344, June 1984.

[13] Lin, C. S., and Hasan, M. M., "Vapor Condensation on Liquid Surface Due to Laminar Jet-Induced Mixing: The Effects of System Parameters," AIAA Paper 90-0354, Jan. 1990.

[14] Grayson, G. D., and Navickas, J., "Interaction between Fluid Dynamic and Thermodynamic Phenomena in a Cryogenic Upper Stage," AIAA Paper 93-2753, Jan. 1993.

[15] Navickas, J., "Prediction of a Liquid Tank Thermal Stratification by a Finite Difference Computing Method," AIAA Paper 88-2917, July 1988.

[16] Lin, C. S., and Hasan, M. M., "Numerical Investigation of The Thermal Stratification in Cryogenic Tanks Subjected to Wall Heat Flux," AIAA Paper 90-2375, July 1990.

[17] Grayson, G. D., Watts, D. A., and Jurns, J. M., "Thermo-Fluid-Dynamic Modeling of a Contained Liquid in Variable Heating and Acceleration Environments," American Society of Mechanical Engineers Paper FEDSM97-3567, June 1997.

[18] Hung, R. J., and Shyu, K. L., "Constant Reverse Thrust Activated Reorientation of Liquid Hydrogen with Geyser Initiation," *Journal of Spacecraft and Rockets*, Vol. 29, No. 2, 1992, pp. 279–285. doi:10.2514/3.26346

[19] Liu, C. H., "A Numerical Calculation of Time Dependant Dynamical Behavior of Liquid Propellants in a Microgravity Environment," *Microgravity Science and Technology*, Vol. 7, No. 2, 1994, pp. 169–172.

[20] Hung, R. J., and Lee, C. C., "Effect of a Baffle on SloshWaves Excited by Gravity-Gradient Acceleration in Microgravity," *Journal of Spacecraft and Rockets*, Vol. 31, No. 6, 1994, pp. 1107–1114. doi:10.2514/3.26566

[21] Peterson, L. D., Crawley, E. F., and Hansman, R. J., "Nonlinear Fluid Slosh Coupled to the Dynamics of a Spacecraft," *AIAA Journal*, Vol. 27, No. 9, 1989, pp. 1230–1240. doi:10.2514/3.10250

[22] Marchetta, J. G., Hochstein, J. I., and Sauter, D. R., "Simulation and Prediction of Magnetic Cryogenic Propellant Positioning in Reduced Gravity," AIAA Paper 2001-0930, Jan. 2001.

[23] Marchetta, J. G., and Hochstein, J. I., "Simulation and Dimensionless Modeling of Magnetically Induced Reorientation," AIAA Paper 2000-0700, Jan. 2000.

[24] Thornton, R. J., and Hochstein, J. I., "Microgravity Propellant Tank Geyser Analysis and Prediction," AIAA Paper 2001-1132, Jan. 2001.

[25] Kothe, D. B., Mjolsness, C. R., and Torrey, M. D., "RIPPLE: A Computer Program for Incompressible Flows with Free Surfaces," Los Alamos National Laboratory LA-12007-MS, Apr. 1991.

[26] Panzarella, C. H., and Kassemi, M., "Self-Pressurization of Large Spherical Cryogenic Tanks in Microgravity," *Journal of Spacecraft and Rockets*, Vol. 42, No. 2, 2005, pp. 299–308. doi:10.2514/1.4571

[27] Panzarella, C., Plachta, D., and Kassemi, M., "Pressure Control of Large Cryogenic Tanks in Microgravity," *Cryogenics*, Vol. 44, No. 7, 2004, pp. 475–48. doi:10.1016/j.cryogenics.2004.03.009

[28] Gresho, P. M., Lee, R. L., and Sani, R. C., "On the Time-Dependent Solution of the Incompressible Navier–Stokes Equations in Two and Three Dimensions," *Recent Advances in Numerical Methods in Fluids*, Pineridge Press, Swansea, England, U.K., Vol. 1, 1979, pp. 27–79.

K. Frendi
Associate Editor